Energy Relaxation of Electrons in InGaN Quantum Wells

BEYZA SARIKAVAK-LISESIVDIN, SEFER BORA LISESIVDIN, NACI BALKAN, GOKHAN ATMACA, POLAT NARIN, HUSEYIN CAKMAK, and EKMEL OZBAY

In this study, electron energy relaxation mechanisms in HEMT structures with different $In_xGa_{1-x}N$-channel quantum well (QW) widths are investigated. Theoretical value of the inelastic scattering rates is carried out at electron temperatures between 30 K (−243 °C) $< T_e <$ 700 K (427 °C). We used both the experimentally determined and calculated electron temperatures to estimate the energy relaxation rates of non-equilibrium electrons. In wide InGaN QWs, power loss of an electron is shown to be significantly smaller than that in the narrower QWs.

DOI: 10.1007/s11661-015-2762-2
© The Minerals, Metals & Materials Society and ASM International 2015

I. INTRODUCTION

OVER the last decade GaN-based heterostructures have been one of the most actively investigated materials because of their outstanding features including large breakdown field and polarization-induced high sheet carrier densities over 10^{13} cm^{-2}[1,2] These coupled with the improvements in the material quality, optoelectronic applications like light emitting diodes (LED), lasers, and sensors have started to be studied extensively.[3,4] $In_xGa_{1-x}N$ alloy has a direct band gap and for the mole fractions ($0 \le x \le 1$), it corresponds to the visible range of the electromagnetic spectrum, It is therefore, one of the most investigated compounds for tandem solar cells, sensors, LEDs, and laser sources.[3–6] Furthermore, high electron mobility transistor (HEMT) structures where an $In_xGa_{1-x}N$-channel with high sheet carrier density and enhanced confinement, inserted between the barrier and GaN layers have huge potential in high power millimeter-wave applications.[7] Also, it has been reported that HEMT structures with $In_xGa_{1-x}N$-channels have improved current collapse behavior with improved low-frequency noise.[8] However, because of its alloy nature, 2DEG is subject to enhanced alloy-disorder scattering.[9] In order to suppress the alloy-disorder scattering, an ultrathin $In_xGa_{1-x}N$-channel has been proposed recently.[10]

In order to evaluate the performance of devices with μm and sub μm dimensions where the application of a few Volts gives rise to electric field in excess of 10^1 kV/cm hot electron transport must be considered.[11] There are number of studies about hot electron transport in the GaN-based heterostructures, especially AlGaN/GaN and AlInN/GaN structures.[12–14] In addition to these studies and possible optoelectronic device applications, it becomes increasingly important to understand the non-equilibrium electron energy and momentum relaxation mechanisms in InGaN quantum wells (QW)s.

In this work, we investigated the dominant scattering mechanisms for HEMT structures with different InGaN QW well widths and with the obtained results, we experimentally and theoretically investigated the electron temperatures (T_e) and energy relaxations of electrons in InGaN QWs.

II. EXPERIMENTAL DETAILS

$Al_{0.83}In_{0.17}N/AlN/GaN/In_{0.1}Ga_{0.9}N/GaN$ HEMT samples were grown on c-face (0001) sapphire substrates in a vertical low-pressure metal–organic chemical vapor deposition (MOCVD) system. The substrates were cleaned with desorption of the unwanted materials at 1323 K (1050 °C) for 15 minutes before epitaxial growth. The growth was started with a 15 nm AlN nucleation layer at a relatively low temperature (LT) of 823 K (550 °C). Then, a nearly 0.3 μm AlN and 2 μm buffer layers were grown at relatively high temperatures of 1323 K to 1348 K (1050 °C to 1075 °C). After the buffer layers, B2705 and B2706 samples were grown with 3 and 8 nm $In_xGa_{1-x}N$ layers that were grown at a temperature of 1018 K (745 °C), resulting In mole fractions of $x = 0.1$. After $In_{0.1}Ga_{0.9}N$ channel layers, a nearly 1 nm LT AlN interlayer, 10 nm LT AlInN barrier layer, and 3 nm GaN cap layer were grown at 1103 K (830 °C). The interlayer is used in order to reduce the alloy-disorder scattering sourced by the barrier layer.[15] Therefore, only alloy-disorder

BEYZA SARIKAVAK-LISESIVDIN, Lecturer, and SEFER BORA LISESIVDIN, Associate Professor, are with the Department of Physics, Faculty of Science, Gazi University, Teknikokullar, 06500 Ankara, Turkey, and also with the School of Computer Science and Electronic Engineering, University of Essex, Wivenhoe Park, Colchester CO4 3SQ, U.K. Contact e-mail: beyzas@gazi.edu.tr NACI BALKAN, Professor, is with the School of Computer Science and Electronic Engineering, University of Essex, and also with the Department of Physics, Faculty of Science, Istanbul University, Vezneciler, 34134 Istanbul, Turkey. GOKHAN ATMACA and POLAT NARIN, Ph.D. Students, are with the Department of Physics, Faculty of Science, Gazi University. HUSEYIN CAKMAK, Research Engineer, is with the Nanotechnology Research Center, Bilkent University, 06800 Bilkent, Ankara, Turkey. EKMEL OZBAY, Professor, is with the Nanotechnology Research Center, Bilkent University, and also with the Department of Physics, Department of Electrical and Electronics Engineering, Bilkent University, 06800 Bilkent, Ankara, Turkey.

Manuscript submitted April 16, 2014.
Article published online 29 January 2015

scattering source is $In_{0.1}Ga_{0.9}N$ QW layer in the studied samples. All the layers were grown undoped.

Temperature dependent [30 K to 300 K (−243 °C to 427 °C)] Hall effect and resistivity measurements were carried out using square shaped (7 × 7 mm^2) samples with Ti/Al/Ni/Au ohmic contacts located at the corners. The magnetic field was kept at B = 4 kg in the Hall effect measurements and zero-field resistivities were used in calculations. The high-speed current–voltage (I–V) characteristics were measured at a lattice temperature of T_L = 30 K (−243 °C) using simple-bar-shaped samples of length l = 4 μm and w = 1 μm. In the I–V measurements, voltage pulses of 20 ns duration with a duty cycle of 0.005 pct were applied along the length of the sample up to a maximum electric field of F = 250 kV/cm. Applied voltage and current through the sample were measured using a computer system equipped with 1 GHz real time oscilloscope. From the I–V measurements drift velocity (v_d) *vs* F plots were obtained with the assumption that the 2DEG electron density within the HEMT structure remains constant within the applied electric field ranges.[16]

III. RESULTS AND DISCUSSION

Figures 1(a) and (b) represent two-dimensional (2D) scattering analyses for the samples B2705 and B2706, respectively. It is clear from the measurements that both samples showed 2D behavior at all temperatures. If we neglect the possibility of parasitic bulk conduction channel (barrier), all the conduction can be assumed to take place in the $In_{0.1}Ga_{0.9}N$ QW. The experimental data were compared with the theoretical calculations which were carried out by taking into account of all the possible momentum scattering mechanisms, namely, polar optical phonon scattering (μ_{PO}),[17] acoustic phonon scattering (μ_{AC}), which includes piezoelectric scattering and deformation potential scattering,[18] alloy-disorder scattering (μ_{Alloy}),[9] interface roughness scattering (μ_{IFR})[19], and background impurity scattering (μ_{IMP}).[20] The details of these scattering mechanisms are discussed elsewhere in detail and not the subject of this study.[21] It is clear from Figure 1 that theoretical mobility agrees well with the experimental results. It is worth noting that the most dominant momentum scattering mechanisms in the sample B2705 are alloy-disorder and interface roughness scattering. The InGaN QW width is considerably wider in sample B2706, alloy-disorder scattering appears to be stronger than in B2705. This is also consistent with the Okamoto *et al.*'s findings about the suppression of alloy-disorder scattering in thinner QWs.[10] In both samples, background impurity scattering is found to be the least effective scattering mechanism at temperatures T_L >150 K (−123 °C). For both samples, polar optical phonon scattering becomes the most effective scattering mechanism nearly after 370 K (97 °C). We used the fit parameters to calculate the total mobility, μ_{Total} up to T_L = 700 K (427 °C).

In Figure 2, pulsed current—applied electric field (I–F) plots for the studied samples are shown at the lattice temperature of T_L = 30 K (−243 °C). For the

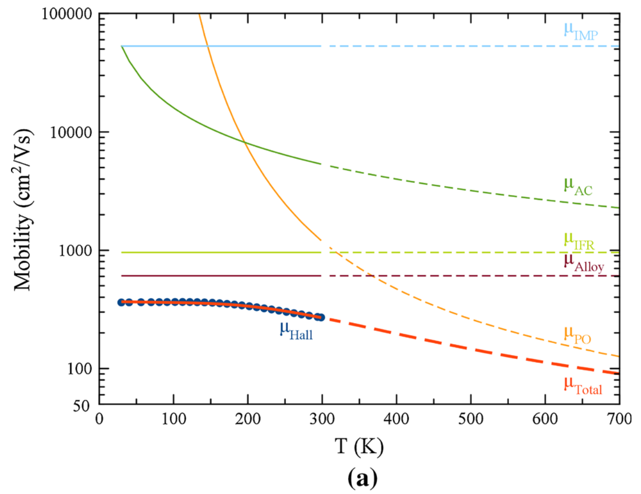

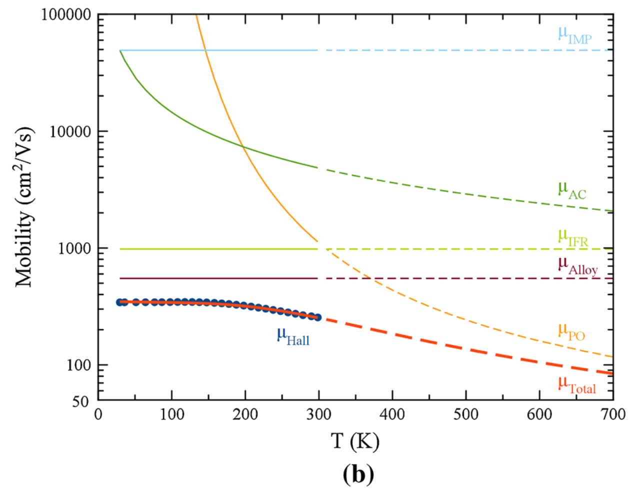

Fig. 1—Momentum scattering analyses in the samples (*a*) B2705 and (*b*) B2706.

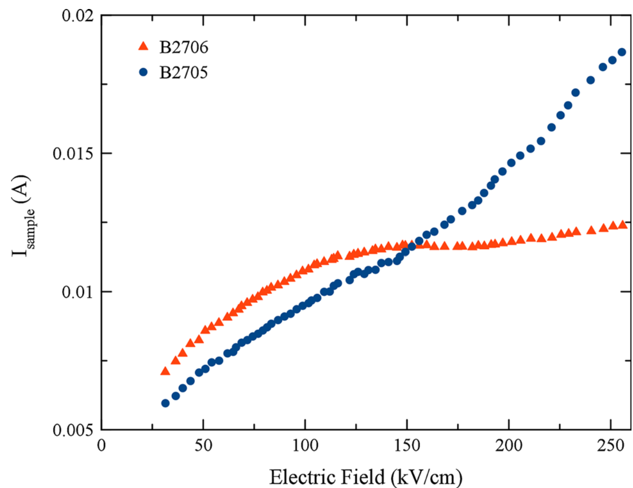

Fig. 2—Pulsed current–applied electric field measurements at lattice temperature, T_L = 30 K (−243 °C).

B2705, the resistance is ohmic at applied electric fields $F < 250$ kV/cm ($V < 100$ V), which is consistent with the previously published results Balkan *et al.*[22] Because

of the suppression of alloy-disorder scattering in thinner QWs, structure behaves like a structure with non-alloyed QW.[10] For B2706, the resistance is ohmic only at applied electric fields of $F < 125$ kV/cm ($V < 50$ V). Saturation of the current at higher electric fields may be a result of the non-suppression of alloy-disorder scattering in a wider InGaN QW in this sample. For B2706, I–F characteristic becomes non-linear at applied electric fields of $F > 125$ kV/cm, because of increased momentum scattering of hot electrons with polar optical phonons. The current saturates at 115 mA at an electric field of F ~175 kV/cm. The plateau is followed by a slight increase with the increasing applied electric field.

In Figure 3, the drift velocity *vs* applied electric field ($v_d - F$) plots are shown for the samples. In sample B2706, which has the wider $In_{0.1}Ga_{0.9}N$ well of the two samples, a drift velocity saturation of around $v_d = 1.0 \times 10^7$ cm/s and at an electric field of $F = 125$ kV/cm was observed. In B2705, with the narrower $In_{0.1}Ga_{0.9}N$ QW the drift velocity increases monotonically without any evidence for saturation up to an applied electric field $F = 250$ kV/cm.

In order to calculate the temperatures of the non-equilibrium electrons, we have used the mobility comparison method, which was also successfully used for bulk GaAs, GaN, InN, and their heterostructures with 2DEG.[12,13,23,24] It is important to point that the accuracy of the mobility comparison method strictly assumes that the sheet carrier density does not change with the applied electric field, the dependence of the momentum relaxation on the electron temperature or electric field is identical to its dependence on the T_L and the non-equilibrium electron distribution can be represented by an electron temperature value which is greater than the T_L. The details of these assumptions that used the mobility comparison method are discussed elsewhere.[22] We plot the lattice temperature dependence of the Hall mobility (μ_H) at very low electric field (F ~1 to 5×10^{-3} kV/cm in this study) and the electric field dependence of the mobility (μ_E) at a fixed lattice temperature [$T_L = 30$ K (−243 °C) in this study] and then compare the two plots, electron temperatures are obtained as a function of the electric field. Because of the experimentally determined μ_H values are measured only up to $T_L = 300$ K (27 °C), we used the μ_{Total} values, calculated at temperatures 300 K (27 °C) < T_L < 700 K (427 °C) as explained above and shown in Figure 1. Thus, we were able to obtain electron temperatures using both the measured and calculated mobilities. The results are shown in Figure 4 with filled markers and lines, respectively. Up to an applied field of $F = 70$ kV/cm, in both samples we see almost identical, nearly, same electron temperatures. With the increasing electric field, however, the electron temperature in the sample with the wider InGaN QW (B2706) increases with the applied field monotonically up to $T_e = 700$ K (427 °C). However, in the sample with the narrower InGaN QW (B2705), the electron temperature saturates at $T_e = 600$ K (327 °C).

The power balance equations in the steady state were used to calculate the energy loss rates that can be obtained as a function of electric field *via* Eqs. [1] and [2]

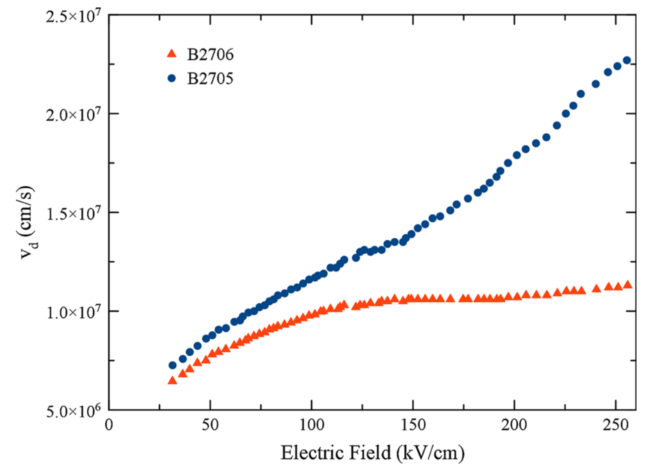

Fig. 3—Electron drift velocity *vs* applied electric field measured at lattice temperature, $T_L = 30$ K (−243 °C).

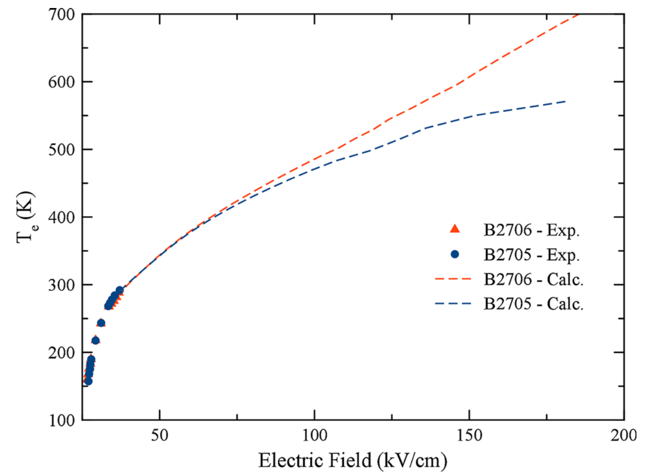

Fig. 4—Electron temperature *vs* applied electric field at lattice temperature of $T_L = 30$ K (−243 °C). Experimental and calculated values are shown with filled markers and dashed lines, respectively.

below. The power gained per electron from the external field[25] equals to the power loss by an electron by inelastic scattering,

$$p = e\mu_F F^2, \quad [1]$$

where p, μ_F are rate of energy and mobility at electric field F, respectively. In Figure 5, the experimental power loss per electron values at $T_L = 30$ K (−243 °C) were plotted as a function of electron temperature using Eq. [1] with the help of Figure 4. Also, the power loss involving the emission and absorption of longitudinal polar optical phonons, which is in form[25]

$$p = \frac{\hbar\omega_{PO}}{k_B T_e}\left[e^{-\hbar\omega_{PO}/k_B T_e} - e^{-\hbar\omega_{PO}/k_B T_L}\right], \quad [2]$$

is shown in the figure for $In_{0.1}Ga_{0.9}N$ alloy as a full line. Here, ε_∞, ε_s, τ_0, $\hbar\omega_{PO}$ are high-frequency and static permittivities, the time constant for longitudinal polar

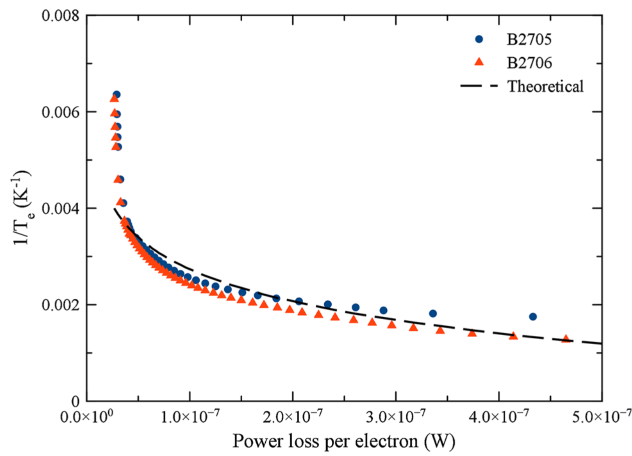

Fig. 5—Experimental power loss per electron *vs* inverse electron temperature (filled markers). Continuous line is the theoretical power loss obtained from Eq. [2].

optical phonon scattering and the polar optical phonon energy, respectively. We used a scattering time of $\tau_0 = 8$ fs, which can be calculated with Fröhlich coupling constant.[13] It is clear from the Figure 1 that the temperature-dependent electron mobilities of both samples are limited with scattering by LO phonons at temperatures above 370 K (97 °C). Therefore, it can be assumed that, for electron temperatures of $T_e > 370$ K (97 °C), longitudinal polar optic phonon scattering is also the dominant energy loss mechanism. In the studied electron temperature range, B2706 shows lower power loss values than the B2705 for any electron temperature. For B2706, the experimental power loss rate is lower than the theoretical value in the studied electron temperature range. This behavior of the B2706 is expected to occur in samples where the free carrier density decreases with increasing electric field. It may also be associated with the hot phonon production at higher electric fields,[13,26] which is not included in mobility comparison method. Hot phonon production can also explain the saturation of the drift velocity of the sample B2706.[27] For B2705, the experimental power loss slope shows a difference that is more evident at low electron temperatures. This shows that the contribution of acoustic phonon emission to the relaxation processes may be comparable to the longitudinal polar optical phonon emission.

IV. CONCLUSIONS

With the help of temperature-dependent Hall mobility and analytic expressions for relevant scattering mechanisms, temperature-dependent electron mobility of GaN-based HEMT structures with different InGaN QW widths are calculated up to $T = 700$ K (427 °C). Electric field-dependent mobilities are also calculated using high field current—electric field measurements up to an applied field of $F = 250$ kV/cm. Electric field-dependent electron temperatures are calculated with the help of temperature- and electric field-dependent mobilities. The experimentally determined and theoretical power loss values are calculated. Electrons in the structures with both narrow and wide QW, represent nearly same electron temperature behavior up to 70 kV/cm. With the increasing electric field, however, the structure with the wider QW has higher electron temperatures. The structure with the wider QW shows smaller power loss than the structure with the narrower QW at a given electron temperature. The structure with thicker InGaN QW shows power loss behavior which may be related to decreasing free carrier density by increasing electric field or hot phonon production at higher electric fields. In the structure with narrower QW at temperatures $T < 370$ K (97 °C), energy relaxation occurs by a mixture of both inelastic scattering by acoustic phonons and longitudinal polar optical phonons.

ACKNOWLEDGMENTS

This work is supported by the State Planning Organization of Turkey under Grant No. 2001K120590, by the European Union under the projects EU-PHOME and EU-ECONAM, and TUBITAK under the Project Nos. 106E198, 107A004, 107A012, and 113F277. One of the authors (Ekmel Ozbay) acknowledges partial support from the Turkish Academy of Sciences. Authors, (Beyza Sarikavak-Lisesivdin and Sefer Bora Lisesivdin) acknowledge partial support from the TUBITAK 2219 numbered scholarships. We would like to thank the NANOTAM engineers for their help.

REFERENCES

1. M.A. Khan and M.S. Shur: *Mater. Sci. Eng. B*, 1997, vol. 46 (1), pp. 69–73.
2. S.N. Mohammad and H. Morkoç: *Prog. Quant. Electron.*, 1996, vol. 20 (5), pp. 361–525.
3. S. Nakamura, S. Pearton, and G. Fasol: *The Blue Laser Diode: The Complete Story*, Springer, Berlin, 2000.
4. S.K. Patra, S. Adhikari, and S. Pal: *J. Disp. Technol.*, 2013, vol. 9 (5), pp. 339–45.
5. S.X. Li, R.E. Jones, E.E. Haller, K.M. Yu, W. Walukiewicz, J.W. Ager, Z. Liliental-Weber, H. Lu, and W.J. Schaff: *Appl. Phys. Lett.*, 2006, vol. 88 (15), p. 151101.
6. A. Pesach, E. Gross, C.-Y. Huang, Y.-D. Lin, A. Vardi, S.E. Schacham, S. Nakamura, and G. Bahir: *Appl. Phys. Lett.*, 2013, vol. 103 (2), p. 022110.
7. G. Simin, X. Hu, A. Tarakji, J. Zhang, A. Koudymov, S. Saygi, J. Yang, M.A. Khan, M.S. Shur, and R. Gaska: *Jpn. J. Appl. Phys.*, 2001, vol. 40 (11A), p. L1142.
8. N. Pala, S. Rumyantsev, M. Shur, R. Gaska, X. Hu, J. Yang, G. Simin, and M. Asif Khan: *Solid State Electron.*, 2003, vol. 47 (6), pp. 1099–1104.
9. M.J. Kearney and A.I. Horrell: *Semicond. Sci. Technol.*, 1998, vol. 13 (2), pp. 174–80.
10. N. Okamoto, K. Hoshino, N. Hara, M. Takikawa, and Y. Arakawa: *J. Cryst. Growth*, 2004, vol. 272 (1), pp. 278–84.
11. B.E. Foutz, S.K. O'Leary, M.S. Shur, and L.F. Eastman: *J. Appl. Phys.*, 1999, vol. 85 (11), pp. 7727–34.
12. B.A. Danilchenko, S.E. Zelensky, E. Drok, S.A. Vitusevich, S.V. Danylyuk, N. Klein, H. Lüth, A.E. Belyaev, and V.A. Kochelap: *Appl. Phys. Lett.*, 2004, vol. 85 (22), pp. 5421–23.

13. D. Zanato, N. Balkan, G. Hill, and W.J. Schaff: *Superlattices Microstruct*., 2004, vol. 36 (4), pp. 455–63.
14. A. Matulionis, J. Liberis, E. Šermukšnis, J. Xie, J.H. Leach, M. Wu, and H. Morkoç: *Semicond. Sci. Technol*., 2008, vol. 23 (7), p. 075048.
15. I.P. Smorchkova, L. Chen, T. Mates, L. Shen, S. Heikman, B. Moran, S. Keller, S.P. DenBaars, J.S. Speck, and U.K. Mishra: *J. Appl. Phys*., 2001, vol. 90 (10), pp. 5196–5201.
16. B.K. Ridley, W.J. Schaff, and L.F. Eastman: *J. Appl. Phys*., 2004, vol. 96 (3), pp. 1499–1502.
17. B.K. Ridley: *J. Phys. C Solid State Phys*., 1982, vol. 15 (28), pp. 5899–5917.
18. B.K. Ridley, B.E. Foutz, and L.F. Eastman: *Phys. Rev. B*, 2000, vol. 61 (24), pp. 16862–69.
19. D. Zanato, S. Gokden, N. Balkan, B.K. Ridley, and W.J. Schaff: *Semicond. Sci. Technol*., 2004, vol. 19 (3), pp. 427–32.
20. K. Hess: *Appl. Phys. Lett*., 1979, vol. 35 (7), pp. 484–86.
21. S.B. Lisesivdin, A. Yildiz, N. Balkan, M. Kasap, S. Ozcelik, and E. Ozbay: *J. Appl. Phys*., 2010, vol. 108 (1), p. 013712.
22. N. Balkan, M.C. Arikan, S. Gokden, V. Tilak, B. Schaff, and R.J. Shealy: *J. Phys. Condens. Matter*, 2002, vol. 14 (13), pp. 3457–68.
23. R. Gupta, N. Balkan, and B.K. Ridley: *Semicond. Sci. Technol*., 1992, vol. 7 (3B), pp. B274–78.
24. D. Zanato, N. Balkan, B.K. Ridley, G. Hill, and W.J. Schaff: *Semicond. Sci. Technol*., 2004, vol. 19 (8), pp. 1024–28.
25. B.K. Ridley: *Semicond. Sci. Technol*., 1989, vol. 4 (12), pp. 1142–50.
26. Y. Sun, M.P. Vaughan, A. Agarwal, M. Yilmaz, B. Ulug, A. Ulug, N. Balkan, M. Sopanen, O. Reentilä, M. Mattila, C. Fontaine, and A. Arnoult: *Phys. Rev. B*., 2007, vol. 75 (20), p. 205316.
27. C. Bulutay and B.K. Ridley: *Superlattices Microstruct*., 2004, vol. 36 (4), pp. 465–71.